Compliant Actuation of Rehabilitation Robots

©PUNCHSTOCK

Benefits and Limitations of Series Elastic Actuators

BY HEIKE VALLERY, JAN VENEMAN, EDWIN VAN ASSELDONK, RALF EKKELENKAMP, MARTIN BUSS, AND HERMAN VAN DER KOOIJ

Digital Object Identifier 10.1109/MRA.2008.927689

Development of robotic devices for gait rehabilitation of stroke patients is motivated by the need for a both intensive and task-specific training, which are key factors in recovery [1], [2], and by the need for therapist-friendly training. Evaluations of the first-generation commercial devices have shown that gait training using these devices is at least as effective as manual therapy [3], [4]. First-generation devices are characterized by the approach of enforcing gait upon a patient by rigidly moving the legs through a prescribed pattern, so that the patient can hardly influence these motions. The training effect may be extendable by increasing active participation of patients, e.g., by letting the patient walk on own effort and only offer robotic assistance as needed (AAN). The potential of AAN algorithms in promoting neural recovery has not yet been shown in gait training of humans, but it was assessed in gait training of mice [5] and in arm training of stroke patients [6], [7]. AAN strategies require interaction control [8], meaning that the apparent mechanical impedance of the device is programmable to desired values (within limits), so that the behavior of the robot can be varied from very stiff to very compliant. Compared with general haptic devices, low apparent stiffness and mass are demanded from a gait trainer, and gait motions are slow. We opted for a combination of compliant actuation and impedance control [9], [10], which provides means to minimize undesired interaction torques.

This article describes and discusses the general advantages and limitations of a compliant actuation concept for rehabilitation robots on the example of our realization called the lower extremity powered exoskeleton (LOPES). The major focus is on the limitations: stiffness and bandwidth constraints as well as the influence of uncompensated exoskeleton dynamics. The stability analysis provides an interesting new result. If the rendered stiffness of an elastically actuated joint is increased beyond the intrinsic stiffness of the elastic element, stability of the coupled system human-robot cannot be guaranteed, at least not in the conservative terms of passivity. Finally, the experimental results with subjects walking with the device are presented. These results show that the limitations, in the given application, become secondary to the gain of compliant actuation.

LOPES: A Low-Weight Exoskeleton with Series Elastic Actuated Joints

Mechanical Design

Impedance control implies that the actuators should be high-precision force sources. Mass and inertia of the actuated construction (the exoskeleton) should be minimized, as the means to reduce the apparent mass by control are limited. Our gait rehabilitation robot LOPES is characterized by 1) the choice of degrees of freedom (DoF) that are actuated or left free to allow kinematically natural walking patterns and 2) the possibility

1070-9932/08/$25.00©2008 IEEE

Authorized licensed use limited to: National Chung Hsing University. Downloaded on June 03,2010 at 07:55:47 UTC from IEEE Xplore. Restrictions apply.

of low impedance control of these DoF to allow unhindered and thus kinetically natural walking. Both horizontal pelvis translations are actuated [1 and 2 in Figure 1(a)]; the vertical motion of the pelvis is left free with passive weight compensation [3 in Figure 1(a)]. There are three rotational joints per leg: hip adduction [4 in Figure 1(a)], hip flexion [5 in Figure 1(a)], and knee flexion [6 in Figure 1(a)]. With these nine DoF, LOPES allows more versatile motion than just forward stepping (as also provided by commercial devices such as the Lokomat [11]). Maintaining the fundamental instability of a standing or walking human, LOPES allows balance training, which has been recognized as an important aspect of gait training [12], [13]. Pelvis motion is also increasingly integrated into other new robotic devices such as ALEX [14] or KineAssist [15].

In contrast to the aforementioned devices, which use stiff actuators, LOPES is intrinsically compliant, similar to PAM and POGO presented in [8]. The joints of the robot are actuated with series elastic actuators (SEAs), an actuation principle introduced by Robinson and colleagues [16]. Bowden cables are used to realize a flexible transmission, so that the motors are detached from the exoskeleton, reducing its weight [see Figure 1(a)]. For the rotary joints, two compression springs are connected to the actuator disk with a cable, so that a torsion spring is created between the actuator disk and the load side segment [see Figure 1(b)]. Both springs are pretensioned with the maximum desired force, so that the cables are always under tension during operation. The concept, construction, and functionality of these joints are described extensively in [9]. The sideways pelvis translation is equipped with a linear SEA.

Table 1 provides the geometric and inertial specifications of the exoskeleton part. For each segment of the exoskeleton, the length L, the center of mass location with respect to the proximal joint L_{CoM}, the mass m, and the moment of inertia around the center of mass J_{s1} and around the proximal joint J_{s2} are listed for an average configuration (the segment lengths are adaptable to the patient). Table 2 gives the specifications of components used in the actuation part. Motor and gear inertial properties and transmission ratio i determine the reflected inertia J_A or m_A of the drives in the exoskeleton coordinate system. For the sideways direction, the reflected mass m_A of the drive is 1.2 kg, much less

To lower undesired interaction torques, it is crucial to minimize the reflected mass of the device.

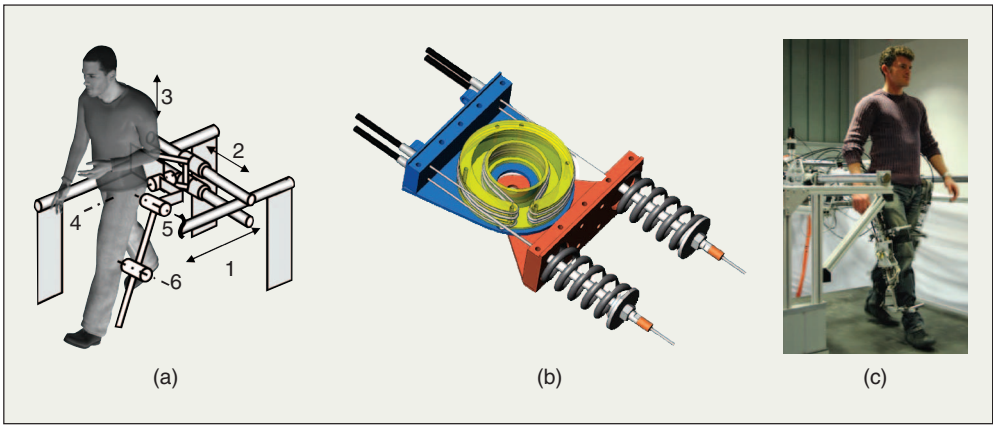

Figure 1. *Design of the LOPES robot. (a) DoF of the pelvis and leg segments of the LOPES gait rehabilitation robot: (1) forward linear guides, (2) sideways linear guides, (3) vertical motion, passively weight compensated by a spring parallelogram between frame and pelvis segment, (4) hip frontal rotation (adduction), (5) hip sagittal rotation (flexion/extension), (6) knee sagittal rotation. Except for (3), all DoFs are actuated. (b) Design of the SEAs: Bowden cables connect the springs to EM motors, which are detached from the exoskeleton. (c) Photographic impression of LOPES in operation.*

Table 1. Dimensions and mass properties of the LOPES exoskeleton.

	L (m)	L_{CoM} (m)	m (kg)	J_{s1} (kg·m²)	J_{s2} (kg·m²)
Upper limb	0.43	0.27	2.9	0.088	0.30
Lower limb	0.37	0.17	2.25	0.064	0.13
Pelvis B/F			35		
Pelvis L/R			27		

Table 2. Actuator specifications of the LOPES.

DoF	Motor Type	Power	Torque/ Force	Motor Inertia	Gear Inertia	i	Refl. Inertia J_A, m_A	r_d	k_s
Flex/ext hip	Kollmorgen	567 W	2.73 Nm	1.6e-5 kg · m²	1.6e-5 kg · m²	64	0.13 kg · m²	0.047 m	35.10 kN/m
Flex/ext knee	Kollmorgen	567 W	2.73 Nm	1.6e-5 kg · m²	1.6e-5 kg · m²	64	0.13 kg · m²	0.047 m	35.10 kN/m
Ab/ad hip	Kollmorgen	567 W	2.73 Nm	1.6e-5 kg · m²	1.6e-5 kg · m²	64	0.13 kg · m²	0.047 m	57.20 kN/m
Left/right	Berger-Lahr	690 W	2.2 Nm	1.6e-4 kg · m²	1.8e-5 kg · m²	$8/r_d$	1.2 kg	0.098 m	3.98 kN/m
Back/forward	Linmot	250 W	204 N	1.8e-5 kg · m²	2.3 kg		2.3 kg		

Authorized licensed use limited to: National Chung Hsing University. Downloaded on June 03,2010 at 07:55:47 UTC from IEEE Xplore. Restrictions apply.

The SEA cannot display a higher pure stiffness than the spring stiffness, if passivity is desired.

than the mass of the pelvis segment (27 kg). In contrast, the reflected moment of inertia J_A of the drives actuating the rotational joints is $0.13\ \mathrm{kg}\cdot\mathrm{m}^2$, which is in the same order of magnitude as the moment of inertia J_{s2} of the exoskeleton segments. However, as the motor mass is decoupled from the exoskeleton by the springs, the actuator mass is not felt by the subject, and the reflected mass of the device is reduced to the exoskeleton mass only. The disk radius r_d and the spring constant k_s in Table 2 define the intrinsic rotational stiffness K of the SEA; for hip and knee, K is given by $2k_s r_d^2 = 155$ Nm/rad.

Control Scheme

The control strategy is multilayered. On the outermost layer, references for the desired interaction with the patient are defined. Two different strategies have been implemented on the LOPES: complementary limb motion estimation (CLME) [17], [18] and virtual model control (VMC) [19], [20]. The control schemes differ in their conceptual background, yet they both aim at improved patient cooperativeness and do not prescribe fixed trajectories to be tracked. This article describes only VMC. The low-level control deals with the SEA unit used to generate and measure the interaction forces. First, this underlying low-level SEA control is described as a single-input single-output (SISO) system, and then, the VMC is outlined.

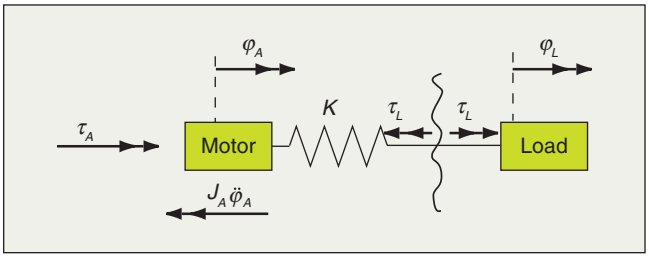

Figure 2. *SEA: The drive is connected to the load via a compliant element (a torsion spring with spring constant K). The drive dynamics are represented by the inertia J_A, and the motor torque is τ_A. The spring torque τ_L acting on the load is proportional to the difference between motor angle φ_A and joint angle φ_L, which makes the spring length a direct measure of the torque acting on the load.*

Control of the SEA

In a SEA, the load is coupled to the drive via a compliant element, in this case, a spring with linear characteristic [see Figure 1(b)]. A relative displacement of load and actuator provokes a spring torque τ_L. This principle is schematically illustrated in Figure 2. The simplifying assumptions made here neglect several important aspects of the actuator side that are relevant in the specific mechanical realization, such as friction and elasticity in the Bowden cable transmission. We justify this by the purpose of the investigations in the later analysis, which is to show some generic parameter and performance limitations of SEAs.

Figure 3 shows the block chart of the SEA embedded in a SISO impedance control loop. The concept of a cascaded force control loop with proportional-integral (PI) controllers was chosen because of its reported effectiveness [21], [22]. In our setup, the innermost motor velocity loop is realized by the pulse-width modulation. The force control has been described and evaluated in [23]. The outer impedance controller sets the desired impedance, whereby we consider only the case of a rendered stiffness P.

Selective and Partial Support of Gait Functions with Virtual Model Control

The observation of manual physical therapy of stroke survivors shows that in case of severely impaired subjects, two or three therapists are needed. Depending on the individual impairment, the therapist assists only in certain gait subtasks. The idea of the LOPES control is that the therapist still decides how to assist the patient but that the strenuous labor is taken over by the robot. Following this concept, LOPES should assist a patient only when it is needed. For example, in case of deficient foot clearance during the swing phase, LOPES should help in lifting up the foot. We have divided the control of human gait into different functional units, which can be partially and selectively supported by LOPES, depending on the patient's individual needs:

1) balance control in the sagittal/frontal plane
2) control of walking speed
3) foot placement in the sagittal and frontal plane

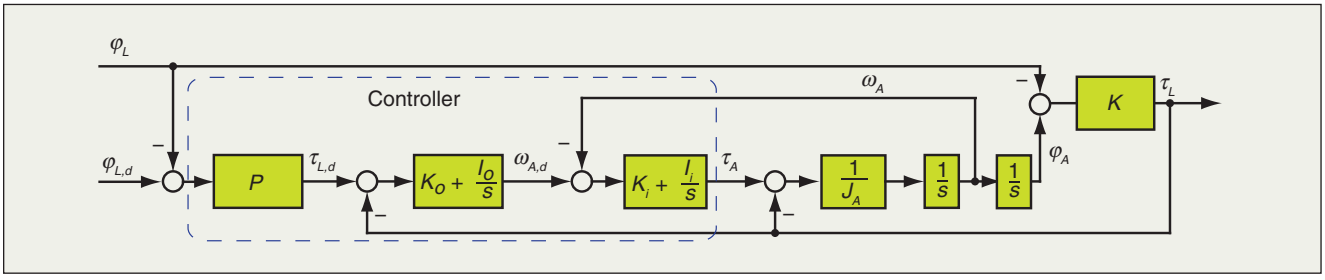

Figure 3. *Impedance control with cascaded torque control. The plant (SEA, on the right) is characterized by actuator inertia J_A and spring constant K. The torque controller is cascaded, with inner (index i) loop on motor velocity ω_A and outer (index o) loop on torque τ_L, both PI-controlled with gains K and I. Outside, an impedance control loop is closed on the joint angle φ_L, here rendering a pure virtual stiffness P. The subscript d denotes reference signals.*

Authorized licensed use limited to: National Chung Hsing University. Downloaded on June 03,2010 at 07:55:47 UTC from IEEE Xplore. Restrictions apply.

4) foot clearance during swing phase to prevent stumbling
5) weight bearing.

The reason behind the division of subfunctions is given in [24]. To support these gait functions, we use VMC, which is a motion control framework that uses virtual mechanical components to generate desired interaction forces and torques. With components such as springs and dampers, it is possible to simulate almost any interaction that a therapist would have with a patient. Usual therapist interaction forces have been quantified in [25]. VMC has been implemented in several two- and three-dimensional walking robot models [26].

The supportive forces for balance control and walking speed control are realized by the drives actuating the pelvis in the horizontal plane [1 and 2 in Figure 1(a)]. All other DoF are rotational, such that the virtual forces in Cartesian space need to be mapped to joint torques. These torques create the illusion that the simulated components are connected to the robot.

Balance control, control of walking speed, and weight bearing are described elsewhere. In this article, we consider only the case of a healthy subject walking in LOPES while the step length and height are modified by VMC. Each of these two virtual models consists of a spring attached to the ankle of LOPES either horizontally or vertically. The desired virtual force acting on the ankle is given by

$$\boldsymbol{F}^{\mathrm{VMC}} = \mathbf{K}_x^{\mathrm{VMC}}(\boldsymbol{x} - \boldsymbol{x}_{\mathrm{ref}}), \tag{1}$$

where $\boldsymbol{K}_x^{\mathrm{VMC}}$ is the Cartesian virtual stiffness matrix, $\boldsymbol{x}$ contains the Cartesian coordinates of LOPES' ankle position, and $\boldsymbol{x}_{\mathrm{ref}}$ is the ankle position reference trajectory. This reference trajectory is tailored to each patient's individual needs, by scaling his/her normal, unassisted ankle trajectory during swing phase in the vertical and horizontal direction to increase foot clearance and/or step length.

The virtual force $\boldsymbol{F}^{\mathrm{VMC}}$ is mapped to joint torque by

$$\tau^{\mathrm{VMC}} = \mathbf{J}^T(\boldsymbol{\theta})\boldsymbol{F}, \tag{2}$$

where $\boldsymbol{\theta}$ is the joint angle and $\mathbf{J}(\boldsymbol{\theta})$ is the Jacobian relating joint velocities to Cartesian ankle velocities. Security measures are taken to avoid knee hyperextension. For step height modification, the ankle height reference is defined with respect to the horizontal ankle-hip distance. Thus, it is not predefined in time. For step length control, the horizontal ankle reference is defined in time, and it is triggered at toe off. Toe off and heel contact are sensed by force transducers on the treadmill.

Advantages of the SEA

Table 3 lists the advantages and drawbacks of SEA. One important advantage is that it allows treating the force control loop as a position control, because the spring length can be considered proportional to the force output. As has previously been demonstrated, a higher compliance in the force control loop allows for higher control gains [16]. This way, better force tracking performance can be achieved. Higher gains allow the realization of proper feedback-controlled torque actuators for LOPES despite substantial adverse effects of high friction and stick-slip in the Bowden cables, as well as play in the transmission. The low realizable impedance of the LOPES robot in the presence of these heavy nonlinear effects has been demonstrated in practical experiments, for example in [23]. Another important advantage of a SEA, as mentioned earlier, is that the spring decouples the motor inertia from the exoskeleton. The Bowden cables also locally decouple the motors from the exoskeleton, further reducing the reflected mass of the device. This reduction is important given that the endpoint mass is an uncontrollable element, i.e., no causal controller can affect its value [27].

A compliantly actuated robot will give way at impact. This is advantageous in terms of safety issues and actuator impact resistance, as well as for realistic stepping experience and training efficacy during impact-type events such as heel strike.

There is a tradeoff between achievable stiffness and low undesired interaction torques.

Performance Limitations

The SEA gains easier and robust force control without depending on expensive (high-speed, high-precision) mechatronic components, yet there is a price to pay. The following analysis will first illustrate the well-known drawback of bandwidth limitations in a compliant actuator [28]. Then, a new result will be presented: the rendered stiffness of the device cannot be increased beyond the stiffness of the elastic element, if conservative demands for stability (in terms of passivity) are to be met. The analysis concludes with the influence of these limitations, as well as the influence of uncompensated exoskeleton mass, on the VMC performance.

Bandwidth Limitations

Bandwidth limitations will be illustrated on the example of the LOPES actuators, first for the SEA alone and then for the more realistic case, in which there is an extra end-effector mass (an exoskeleton) between the patient and the elastic element.

Bandwidth of the SEA with Massless End-Effector

For haptic systems, the impedance Z is generally defined as the transfer of function from the input velocity to the opposing

Table 3. Advantages and disadvantages of SEA.

Pros	Cons
Decoupled actuator inertia	Limited stiffness
Reduction of friction effects	Limited bandwidth
Inherent safety and impact resistance	Extra mechanical element
Energy storage	High power requirements

Authorized licensed use limited to: National Chung Hsing University. Downloaded on June 03,2010 at 07:55:47 UTC from IEEE Xplore. Restrictions apply.

The employed VMC, which attempts to separately modify the selected gait characteristics, proved to be effective.

torque. This definition is used here because it allows to assess stability in terms of passivity. Using the notation of II-B1, $Z(s)$ is

$$Z(s) = \frac{\tau_L}{-\varphi_L s}. \tag{3}$$

With the simplified model of Figure 2, which neglects friction and elasticity of the Bowden cables, and with the parameters given in Figure 3, the impedance transfer function value is

$$Z(s) = \frac{K(J_A s^4 + K_i s^3 + (K_i K_o P + I_i)s^2 + aPs + I_i I_o P)}{(J_A s^4 + K_i s^3 + (K_i K_o K + K + I_i)s^2 + aKs + I_i I_o K)s}, \tag{4}$$

with $a = (I_i K_o + I_o K_i)$.

Replacing the complex variable s in (4) by $j\omega$, the frequency response $Z(j\omega)$ is obtained. A look at the asymptotic behavior of $Z(j\omega)$ is useful for an intuitive understanding of the SEA behavior; for frequencies below the bandwidth ($\omega \to 0$), the programmed impedance can be achieved, which is that of a virtual spring with stiffness P. For high frequencies ($\omega \to \infty$), however, the impedance of the haptic display will approach the impedance of the SEA's mechanical spring with stiffness K.

The integrators show considerable influence only for low frequencies, and thus, the bandwidth analysis can be simplified by considering only the case where both integrator gains are zero. This makes major effects more obvious, as it reduces (4) to

$$Z_s(s) = K\frac{J_A s^2 + K_i s + K_i K_o P}{(J_A s^2 + K_i s + K_i K_o K + K)s}. \tag{5}$$

The actually displayed stiffness value K_{disp} deviates from the value of P if no integrators are employed:

$$K_{\text{disp}} = \lim_{s\to 0} s\ Z_s(s) = \frac{PK_oK_i}{1 + K_oK_i}, \tag{6}$$

and a desired stiffness must be mapped to a higher P.

Figure 4(a) illustrates the bandwidth limitations; for low frequencies, the desired impedance is successfully rendered, whereas for frequencies above the bandwidth, the system behaves like the (stiffer) mechanical spring. For frequencies in between, the behavior approaches a spring-damper, the damping parameter of which depends only on the control parameters (given in the figure legend). The intersection of asymptotes of damper and rendered spring in Figure 4(a) shows that the bandwidth, i.e., the maximum frequency until which rendering of the pure desired stiffness is possible, is bounded by $\omega = PK_o$. This implies that the control gain K_o has a dominant influence on bandwidth. A high value of K_o lowers the damping characteristics of the second-order low-pass in (5), and to counteract this, the motor velocity loop gain value K_i needs to be increased as well. Practical considerations such as motor saturation, however, put bounds on the realizable gains.

Influence of Exoskeleton Mass on Bandwidth

In a realistic rehabilitation robot, there will always be some mass between the actuator and the patient, generally connection elements like an exoskeleton. The exoskeleton LOPES is

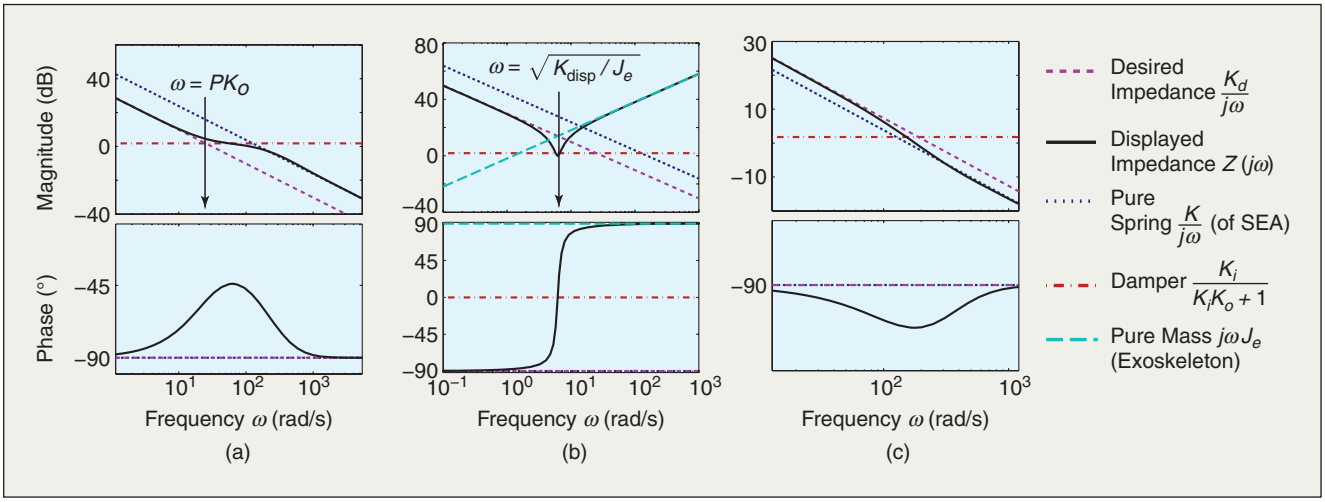

Figure 4. *Bandwidth and stiffness limitations. (a) Bandwidth with massless end effector: At high frequencies, the displayed impedance (black solid line) matches the intrinsic elasticity (green dotted line) of the SEA. The achievable bandwidth depends on the torque control gain K_o. (b) With an additional mass at the load side of the SEA (e.g., an exoskeleton), further bandwidth limitations are introduced. (c) Impedance control with too high desired stiffness (above the natural spring stiffness): The phase of the impedance frequency response has values below −90°, and thus the system is not passive.*

Authorized licensed use limited to: National Chung Hsing University. Downloaded on June 03,2010 at 07:55:47 UTC from IEEE Xplore. Restrictions apply.

constituted of several coupled segments, such that a multi-input multi-output (MIMO) system results. For schematic purposes, i.e., to illustrate the general influence of this extra mass on bandwidth, however, we will consider only the simplified case where a rigid body with inertia J_e is introduced on the load side of the SEA model of Figure 2, which could be interpreted as a 1-DoF exoskeleton. This extra mass augments the impedance transfer function (4) by the extra summand $J_e s$. The system will no longer behave like a spring at high frequencies, and its behavior will then be dominated by the added mass, as displayed in Figure 4(b). Depending on its value, such an additional mass can also lower the bandwidth even further. Another upper bound for the bandwidth is indicated at the intersection of the asymptotes in Figure 4(b), with a value of $\omega = \sqrt{K_{\text{disp}}/J_e}$.

Stiffness Limitations Due to Passivity Concerns

Now, passivity conditions for the impedance control of Figure 3 will be investigated with similar methods as in [23], resulting in bounds for the control gains (with integrators).

Passivity is ensured if the impedance (3) is positive real. Necessary and sufficient conditions for this are as follows [27]:

- $Z(s)$ must be stable
- The real part of $Z(j\omega)$ must be nonnegative for all ω for which $j\omega$ is not a pole of $Z(s)$.

First, we look at the stability condition. As the system poles are independent of the impedance parameters, stability depends only on the inner force control loop. Checking the Hurwitz determinants gives a necessary and sufficient condition:

$$K_i K_o I_i^2 + K K_i (1 + K_o K_i) a - K J_A a^2 > 0. \tag{7}$$

For example, this can be achieved conservatively by following the simple rules in [23], which is to select a velocity loop gain higher than the motor inertia, and constraining both integrator gains to half of the respective proportional gain values.

For passivity, the real part of

$$Z(j\omega) =: A(j\omega)/B(j\omega) \tag{8}$$

has to be nonnegative for all $\omega \in (-\infty, \infty)$ that are not roots of the denominator. For nonzero denominator B, the real part of the complex fraction can be nonnegative only if

$$R(\omega) = \text{Re}(A)\text{Re}(B) + \text{Im}(A)\text{Im}(B) = \sum_{i=1}^{8} d_i \omega^i \tag{9}$$

is nonnegative for all $\omega \in (-\infty, \infty)$. All coefficients d_i of the polynomial in ω are zero, except for

$$d_6 = K\left[(K_i^2 K_o - a J_A)(K - P) + K_i K\right],$$
$$d_4 = K\left[I_i^2 K_o (K - P) - a K P\right].$$

The requirement that both coefficients have to be nonnegative bounds the achievable stiffness. With positive integrator gains, the coefficient d_4 is only nonnegative for

$$P \le K \frac{I_i^2 K_o}{I_i^2 K_o + a K} < K. \tag{10}$$

With zero integrator gains, (9) simplifies to

$$R(\omega) = \omega^6 K(-K_i^2 K_o P + K_i^2 K_o K + K_i K) \ge 0. \tag{11}$$

The controller gain P may thus exceed the value of K. However, without integrators, the stiffness displayed at low frequencies deviates from the value of P, as given in (6), and the actually displayed stiffness K_{disp} equals K for the maximum value of P allowed in (11). This implies that the SEA cannot display a higher pure stiffness than the spring stiffness, if passivity is desired.

It is important to note that the real part of the impedance and thus passivity is independent of the presence of additional end-effector mass J_e, because this simply adds the imaginary term $j\omega J_e$ to the frequency response.

Figure 4(a) and (b) features a desired stiffness lower than the allowed value. The phase never leaves the range of $+90°$ to $-90°$, which is equivalent to a positive real part, and thus the system is passive. In contrast, Figure 4(c) illustrates the case of an excessive desired stiffness; the phase falls below $-90°$. This implies that the haptic display is not passive, and the coupled system will only be stable with a certain number of environments, for example with a pure spring (a differentiator, which shifts the phase up). However, coupled to a pure mass (an integrator), the open-loop frequency response will invariably have a phase below $-180°$ for all frequencies, and thus the closed-loop system is unstable.

Limitations for the VMC

As indicated in the preceding section, both the bandwidth and the maximum value of the rendered stiffness are constrained because of the compliant actuator. Further performance limitations originate from undesired interaction forces due to exoskeleton dynamics. The influence of these effects on the achievable performance of the VMC will now be analyzed.

Performance Limitations Due to Limited Stiffness

To meet passivity requirements, the maximal joint stiffness that can be realized by joint-space impedance control is limited by the spring stiffness of the series elastic element, as was shown in the previous section. This results in boundaries for the maximum displayed Cartesian stiffness, whereby the relation between the Cartesian stiffness matrix $\mathbf{K}_x$ and the joint stiffness matrix $\mathbf{K}_\theta$ is defined by the Jacobian [29]:

$$\mathbf{K}_x = \mathbf{J}^{-T} \mathbf{K}_\theta \mathbf{J}^{-1}. \tag{12}$$

The mapped Cartesian stiffness ellipse, with $\mathbf{K}_\theta$ as the identity matrix and specifications given in Table 1, is displayed in Figure 5. Its shape and orientation are determined by the eigenvalues and vectors of $\mathbf{K}_x$, whereby it can be seen that the smallest eigenvalue depends on the knee angle.

Authorized licensed use limited to: National Chung Hsing University. Downloaded on June 03,2010 at 07:55:47 UTC from IEEE Xplore. Restrictions apply.

When the exoskeleton has 90° knee flexion, the smallest eigenvalue of $\mathbf{K}_x$ is 2.53, and it is 1.3 with 10° knee flexion. The worst case is when the knee is fully extended and when the Cartesian stiffness ellipse is aligned with one of the virtual models. In this worst case scenario, the Cartesian stiffness is only 200 N/m given the maximal joint stiffness of the hip and knee of 155 Nm/rad, as given in the "Mechanical Design" section.

Performance Limitations Due to Manipulator Dynamics

The VMC does not compensate for the open-loop impedance of the exoskeleton. As a consequence, in free space, the human operator will always feel the full inertia and friction of the manipulator [30], and thus not only the virtual model.

The undesired additional interaction torque τ in the swing phase given by the equation of motion of the exoskeleton:

$$\tau = \mathbf{M}(\boldsymbol{\theta})\ddot{\boldsymbol{\theta}} + \mathbf{v}(\boldsymbol{\theta}, \dot{\boldsymbol{\theta}}) + \boldsymbol{g}(\boldsymbol{\theta}), \tag{13}$$

where $\boldsymbol{\theta}$ is the vector of joint angles, $\mathbf{M}(\boldsymbol{\theta})$ is the mass matrix, $\boldsymbol{v}(\boldsymbol{\theta}, \dot{\boldsymbol{\theta}})$ are Coriolis and centrifugal torques, and $\boldsymbol{g}(\boldsymbol{\theta})$ are gravitational torques. To give an idea of the inertia of the device reflected at LOPES's ankle, these unwanted torques can be mapped to forces in Cartesian space with ankle position $\boldsymbol{x}$:

$$\boldsymbol{F} = \mathbf{M}_x(\boldsymbol{\theta})\ddot{\boldsymbol{x}} + \boldsymbol{v}_x(\boldsymbol{\theta}, \dot{\boldsymbol{\theta}}) + \boldsymbol{g}_x(\boldsymbol{\theta}), \tag{14}$$

whereby the relation between joint space and Cartesian space matrices can be derived using the Jacobian [29].

To compensate the components $\boldsymbol{v}_x(\boldsymbol{\theta}, \dot{\boldsymbol{\theta}})$ and $\boldsymbol{g}_x(\boldsymbol{\theta})$, the VMC could be modified, since as terms depend only on joint angles and velocities. However, in our application, we compensate neither of these forces. First, centrifugal and Coriolis forces in $\boldsymbol{v}_x$ are negligibly small. Second, subjects walking with compensated exoskeleton gravitational forces $\boldsymbol{g}_x$ reported that it felt unnatural, and compensating for $\boldsymbol{g}_x$ with constant $\mathbf{M}_x$ increases the natural frequency. (As stated before, $\mathbf{M}_x$ can not be reduced by any causal controller.)

Especially at high frequencies, the behavior of the device is dominated by the reflected mass $\mathbf{M}_x$ of the exoskeleton. With respect to the ankle, this reflected mass is related to the joint space mass matrix by

$$\mathbf{M}_x = \mathbf{J}^{-T}\mathbf{M}\mathbf{J}^{-1}. \tag{15}$$

Using the specifications given in Table 1, this reflected mass is visualized by the inertia ellipse of Figure 5. Its shape and orientation are determined by the eigenvalues and vectors of $\mathbf{M}_x$. The orientation of the ellipse is always perpendicular to the lower segment of the exoskeleton, which means that the reflected mass is minimal in perpendicular direction and maximal in the parallel direction of the most distal segment of the exoskeleton. The eigenvalues of $\mathbf{M}_x$ depend only on the knee angle of the exoskeleton. The smallest eigenvalue remains fairly constant around 0.95 kg. The largest eigenvalue is minimal (3.9 kg) when the knee is 90° flexed and increases when the knee is extended. Note that the reflected mass of the device would be much higher if the motors were not detached from the exoskeleton and if the motor mass was not decoupled from the device by the series elastic element.

Experimental Results

The remarkable capabilities of the SEA in terms of force tracking and backdrivability (i.e., the inner control loop) have been evaluated experimentally and are described in [23]. These practical experiments also showed a very good agreement between the theoretically predicted and actually achieved force tracking bandwidth, with a value of approximately 16 Hz. The experimental results presented in this article are limited to the performance of the outer impedance control loop.

For the control of an individual joint of the exoskeleton alone (without human subject), the maximum achievable stiffness before undesired oscillations occurred is almost equal to the spring stiffness (±10%, depending on gain variations in the torque control loop), as predicted by the theoretical analysis. In contrast, the maximum achievable Cartesian stiffness in practical experiments with healthy subjects walking under the influence of VMC resulted to be 1,500 N/m in vertical direction (step height control) and 700 N/m in horizontal direction (step length control), which is considerably higher than the theoretic worst-case bound. With the angle data from the experiment and (12), the Cartesian stiffness in horizontal direction should be limited to 200 Nm and in vertical direction to 355 Nm.

The reflected mass of the exoskeleton constrains the achievable bandwidth, as illustrated in the "Bandwidth Limitations" section for the SISO case. The limit is given by the square root of the desired stiffness of the virtual component

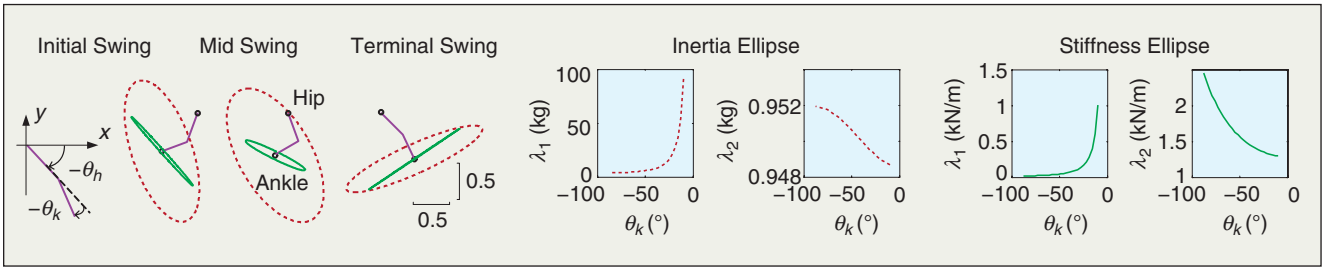

Figure 5. *Reflected mass and stiffness at the ankle: The mass (red and dashed) and stiffness (green and solid) ellipses that reflect the inertia of the exoskeleton and hip and knee joint stiffnesses of 1 Nm/rad at the ankle for different kinematic configurations. The principal axes of the stiffness ellipses are the inverse of the Cartesian stiffness matrix eigenvalues λ_1 and λ_2; the axes of the inertia ellipses are the inverse of the square root of the respective eigenvalues. Thus, the larger the ellipses, the less mass or stiffness is reflected.*

Authorized licensed use limited to: National Chung Hsing University. Downloaded on June 03,2010 at 07:55:47 UTC from IEEE Xplore. Restrictions apply.

divided by the reflected exoskeleton mass. Below this frequency, the virtual spring is felt, whereas above, the reflected device mass is felt. In the case where the reflected mass is minimal (0.95 kg), this frequency is 4.3 and 6.3 Hz for the stiffnesses of 700 and 1,500 N/m, respectively. For a desired stiffness of 700 N/m and using a worst-case approach, it reduces to 2.14, 1.93, 1.21, and 0.44 Hz for 90°, 60°, 30°, and 10° knee flexion, respectively.

Despite these heavy bandwidth limitations, the combination of the mechanical designs of LOPES and VMC was well able to modify the step height and step length of healthy subjects [20]. Each of the two parameters could be lengthened or shortened by VMC, simply by scaling the reference path. The change in each specific gait parameter left the other parts of the gait cycle almost unaffected, and the modification was not perceived awkward until it got excessively large. In experiments with varying stiffness, we found that the subjects perceived stiffer controllers as less comfortable; they preferred more compliant virtual springs. Adjustment of the reference parameters beyond the desired value in combination with a softer controller (equivalent to additional feedforward torques, which is not unique to VMC) also achieved the desired modification and was perceived as more comfortable than a stiff control. The selective modification of average ankle trajectories is shown in Figure 6 for the maximum stiffness. However, the figure also shows that the step length was not exactly modified by the desired 20% due to the compliant interface. The experiments are described in detail in [31].

Discussion

A comparison of the theoretical predictions and the experimental outcome shows good agreement for joint-space impedance control without human subject, but it also shows that the Cartesian stiffness used in the VMC can be higher than the theoretically derived worst-case bound. The fact that this higher stiffness is rendered without stability problems can be explained by several factors. First, the worst case in terms of kinematic configuration hardly occurred in the practical experiments, or at least, the system never remained in this state for long, such that the instable effects might have been transient. Second, passivity is a conservative means of ensuring stability of coupled systems, and a less conservative, explicit MIMO stability analysis could replace it (requiring the exoskeleton, the patient's impedance, the compliant coupling between human and exoskeleton, and the environment to be modeled reliably, which is difficult). Nevertheless, without a human subject, the theoretical and practical results coincided well. Therefore, a probable reason is that the healthy subjects did not behave like pure masses, the worst environment discussed in the section "Stiffness Limitations Due to Passivity Concerns," but formed stabilizing elements in the control loop. This positive contribution might stem from intrinsic and neuronally coordinated stiffness and damping, and it is for example exploited for the control of BLEEX [32]. Although it seemed possible to render higher stiffness for healthy subjects than theoretically derived, we decided not to rely on this effect when working with patients. Instead, we increased the stiffness of the SEA by a factor of 2.5. Equipped with these stiffer springs, LOPES can operate with sufficiently stiff VMC and still remain within the conservative limits resulting from the passivity analysis. Generally, there is a tradeoff between achievable stiffness on the one hand and low undesired interaction torques on the other. One possibility would be to use an adaptive compliance, as suggested by [33], to meet the individual patient's needs.

Conclusion

This article discusses the pros and cons of compliant actuation for rehabilitation robots on the example of LOPES, focusing on the cons. After illustrating the bandwidth limitations, a new result has been derived: if stability in terms of passivity of the haptic device is desired, the renderable stiffness is bounded by the stiffness of the SEA's elastic component.

In practical experiments with the VMC, the aforementioned limitations affected the control performance. Desired gait modifications were not tracked exactly, because the subjects were able to deviate from the prescribed pattern even in the stiffest possible configuration. Despite the limitations, the practical experiments also demonstrated the general effectiveness of the realization. Manipulation of selected gait parameters is possible, whereby other parameters are left unaffected. This high selectivity is made possible by the low level of undesired interaction torques, which is

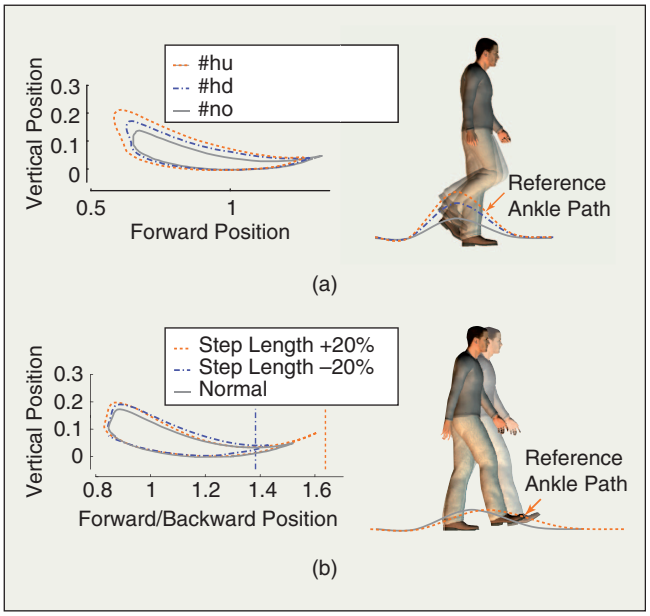

Figure 6. *Modification of the (a) step height and (b) length. The normal ankle trajectories are scaled to obtain a reference trajectory for the ankle. With a virtual spring attached at the ankle, the differences between the true and desired ankle position are mapped to a (a) vertical or (b) horizontal virtual force at the ankle. Typical example of a subject's modified ankle trajectories (a) for the case that the maximal foot clearance is increased to 17 or 22 cm, and (b) for the case that the step length is increased or decreased by 20%.*

Authorized licensed use limited to: National Chung Hsing University. Downloaded on June 03,2010 at 07:55:47 UTC from IEEE Xplore. Restrictions apply.

achieved by elastic decoupling of motor mass and a lightweight exoskeleton.

The discrepancy between theoretical bounds and rendered stiffness indicated that healthy subjects might represent a stabilizing component of the coupled system, which could be different for patients. In light of the theoretical stability analysis and with the focus on patients, the LOPES actuation was slightly modified. The robot was equipped with stiffer springs to obtain sufficient stiffness and to ensure stability without relying on stabilizing effects of the human.

For this application, the disadvantages of compliant actuation can thus be tolerated or dealt with, and they are small compared with the advantages. Given that a rehabilitation robot, in the first place, is supposed to imitate therapist action, the limitations of bandwidth and stiffness do not pose severe problems. In contrast, safety and backdrivability are highly relevant, and they can be ensured easier with a compliant actuator. Therefore, we conclude that compliant actuation and a lightweight exoskeleton provide effective means to accomplish the desired AAN behavior of a rehabilitation robot. The next step is to evaluate the robot behavior, control performance, and therapeutic effectiveness in patient studies.

Acknowledgments

H. Vallery was supported by the Studienstiftung des Deutschen Volkes. All authors from the University of Twente were supported by the Netherlands Organisation for Scientific research (Vernieuwings-impuls 2001, 22016027011, granted to Dr. H. van der Kooij) and by the Institute for Biomedical Technology.

Keywords

Series elastic actuators, gait training, passivity-based control, stroke, compliance, rehabilitation robots.

References

[1] G. Kwakkel, R. C. Wagenaar, T. W. Koelman, G. J. Lankhorst, and J. C. Koetsier, "Effects of intensity of rehabilitation after stroke. A research synthesis," *Stroke*, vol. 28, no. 8, pp. 1550–1556, 1997.

[2] R. Teasell, J. Bitensky, K. Salter, and N. A. Bayona, "The role of timing and intensity of rehabilitation therapies," *Top. Stroke Rehabil.*, vol. 12, no. 3, pp. 46–57, 2005.

[3] B. Husemann, F. Muller, C. Krewer, S. Heller, and E. Koenig, "Effects of locomotion training with assistance of a robot-driven gait orthosis in hemiparetic patients after stroke: A randomized controlled pilot study," *Stroke*, vol. 38, no. 2, pp. 349–354, 2007.

[4] M. Pohl, C. Werner, M. Holzgraefe, G. Kroczek, J. Mehrholz, I. Wingendorf, G. Hoolig, R. Koch, and S. Hesse, "Repetitive locomotor training and physiotherapy improve walking and basic activities of daily living after stroke: A single-blind, randomized multicentre trial (DEutsche GAngtrainerStudie, DEGAS)," *Clin. Rehabil.*, vol. 21, pp. 17–27, 2007.

[5] L. L. Cai, A. J. Fong, C. K. Otoshi, Y. Liang, J. W. Burdick, R. R. Roy, and V. R. Edgerton, "Implications of assist-as-needed robotic step training after a complete spinal cord injury on intrinsic strategies of motor learning," *J. Neurosci.*, vol. 26, no. 41, pp. 10564–10568, 2006.

[6] M. Ferraro, J. J. Palazzolo, J. Krol, H. I. Krebs, N. Hogan, and B. T. Volpe, "Robot-aided sensorimotor arm training improves outcome in patients with chronic stroke," *Neurology*, vol. 61, no. 11, pp. 1604–1607, 2003.

[7] N. Hogan, H. I. Krebs, B. Rohrer, J. J. Palazzolo, L. Dipietro, S. E. Fasoli, J. Stein, R. Hughes, W. R. Frontera, D. Lynch, and B. T. Volpe, "Motions or muscles? Some behavioral factors underlying robotic assistance of motor recovery" *J. Rehabil. Res. Dev.*, vol. 43, no. 5, pp. 605–618, 2006.

[8] D. Aoyagi, W. E. Ichinose, S. J. Harkema, D. J. Reinkensmeyer, and J. E. Bobrow, "A robot and control algorithm that can synchronously assist in naturalistic motion during body-weight-supported gait training following neurologic injury," *IEEE Trans. Neural Syst. Rehab. Eng.*, vol. 15, no. 3, pp. 387–400, 2007.

[9] J. F. Veneman, R. Ekkelenkamp, R. Kruidhof, F. C. T. van der Helm, and H. van der Kooij, "A series elastic- and Bowden-cable-based actuation system for use as torque actuator in exoskeleton-type robots," *Int. J. Robot. Res.*, vol. 25, no. 3, pp. 261–281, 2006.

[10] J. F. Veneman, R. Kruidhof, E. E. G. Hekman, R. Ekkelenkamp, E. H. F. Van Asseldonk, and H. Van der Kooij, "Design and evaluation of the LOPES exoskeleton robot for interactive gait rehabilitation," *IEEE Trans. Neural. Syst. Rehabil. Eng.*, vol. 15, no. 3, pp. 379–386, 2007.

[11] G. Colombo, M. Joerg, R. Schreier, and V. Dietz, "Treadmill training of paraplegic patients using a robotic orthosis," *J. Rehabil. Res. Dev.*, vol. 37, no. 6, pp. 693–700, 2000.

[12] J. F. Israel, D. D. Campbell, J. H. Kahn, and T. G. Hornby, "Metabolic costs and muscle activity patterns during robotic- and therapist-assisted treadmill walking in individuals with incomplete spinal cord injury," *Phys. Ther.*, vol. 86, no. 11, pp. 1466–1478, 2006.

[13] D. J. Reinkensmeyer, D. Aoyagi, J. L. Emken, J. A. Galvez, W. Ichinose, G. Kerdanyan, S. Maneekobkunwong, K. Minakata, J. A. Nessler, R. Weber, R. R. Roy, R. de Leon, J. E. Bobrow, S. J. Harkema, and V. R. Edgerton, "Tools for understanding and optimizing robotic gait training," *J. Rehabil. Res. Dev.*, vol. 43, no. 5, pp. 657–670, 2006.

[14] S. K. Banala, S. K. Agrawal, and J. P. Scholz, "Active leg exoskeleton (ALEX) for gait rehabilitation of motor-impaired patients," in *Proc. IEEE ICORR 2007*, pp. 401–407.

[15] M. Peshkin, D. A. Brown, J. J. Santos-Munné, A. Makhlin, E. Lewis, J. E. Colgate, J. Patton, and D. Schwandt, "KineAssist: A robotic overground gait and balance training device," in *Proc. IEEE ICORR 2005*, Chicago, pp. 241–246.

[16] D. W. Robinson, "Design and analysis of series elasticity in closed-loop actuator force control," Ph.D. thesis, Dept. Mech. Eng., MIT, Cambridge, MA, 2000.

[17] H. Vallery and M. Buss, "Bewegungsintentionsschätzung auf Basis von Gelenkkoordination," *at-Automatisierungstechnik*, vol. 55, no. 10, pp. 503–510, 2007.

[18] H. Vallery, R. Ekkelenkamp, H. van der Kooij, and M. Buss, "Complementary limb motion estimation based on interjoint coordination: experimental evaluation," in *Proc. IEEE ICORR 2007*, pp. 798–803.

[19] R. Ekkelenkamp, J. Veneman, and H. van der Kooij, "LOPES: Selective control of gait functions during the gait rehabilitation of CVA patients," in *Proc. IEEE ICORR 2005*, pp. 361–364.

[20] E. H. F. Van Asseldonk, R. Ekkelenkamp, J. F. Veneman, F. C. T. van der Helm, and H. van der Kooij, "Selective control of a subtask of walking in a robotic gait trainer(LOPES)," in *Proc. IEEE ICORR 2007*, pp. 841–848.

[21] G. Wyeth, "Control issues for velocity sourced series elastic actuators," in *Proc. Australasian Conf. Robotics and Automation*, 2006.

[22] G. A. Pratt, P. Willisson, C. Bolton, and A. Hofman, "Late motor processing in low-impedance robots: Impedance control of series-elastic actuators," in *Proc. 2004 ACC*, pp. 3245–3251.

[23] H. Vallery, R. Ekkelenkamp, H. van der Kooij, and M. Buss, "Passive and accurate torque control of series elastic actuators," in *Proc. IEEE IROS 2007*, San Diego, CA, pp. 3534–3538.

[24] H. van der Kooij, R. Jacobs, B. Koopman, and F. van der Helm, "An alternative approach to synthesizing bipedal walking," *Biol. Cybern.*, vol. 88, no. 1, pp. 46–59, 2003.

Authorized licensed use limited to: National Chung Hsing University. Downloaded on June 03,2010 at 07:55:47 UTC from IEEE Xplore. Restrictions apply.

[25] J. A. Galvez, G. Kerdanyan, S. Maneekobkunwong, R. Weber, M. Scott, S. J. Harkema, and D. J. Reinkensmeyer, "Measuring human trainers' skill for the design of better robot control algorithms for gait training after spinal cord injury," in *Proc. IEEE ICORR 2005*, pp. 231–234.

[26] J. E. Pratt, C. M. Chew, A. Torres, P. Dilworth, and G. Pratt, "An intuitive approach for bipedal locomotion," *Int. J. Robot. Res.*, vol. 20, no. 2, pp. 129–143, 2001.

[27] J. E. Colgate, "The control of dynamically interacting systems," Ph.D. thesis, Dept. Mech. Eng., MIT, Cambridge, MA, 1988.

[28] S. D. Eppinger and W. P. Seering, "Understanding bandwidth limitations in robot force control," in *Proc. ICRA 1987*, pp. 904–909.

[29] J. J. Craig, *Introduction to Robototics: Mechanics and Control*, 2nd ed. Reading, MA: Addison-Wesley, 1989.

[30] R. W. Adams and B. Hannaford, "Control Law Design for Haptic Interfaces to Virtual Reality," *IEEE Trans. Contr. Syst. Technol.*, vol. 10, no. 1, pp. 3–13, 2002.

[31] R. Ekkelenkamp, E.H.F. van Asseldonk, B. Koopman, P. H. Veltink, S. Stramigioli, and H. van der Kooij, "Swing phase adaptation during walking by virtual model control of a powered exoskeleton," submitted for publication.

[32] H. Kazerooni, Jean-Louis Racine, Lihua Huang, and Ryan Steger, "On the control of the berkeley lower extremity exoskeleton (BLEEX)," in *Proc. IEEE ICRA 2005*, pp. 4364–4371.

[33] K. W. Hollander, T. G. Sugar, and D. E. Herring, "Adjustable robotic tendon using a 'Jack Spring'," in *Proc. IEEE ICORR 2005*, pp. 113–118.

Heike Vallery received her diploma (with honors) in mechanical engineering from RWTH Aachen University in Germany in 2004. She is about to finish her Ph.D. degree at the Institute of Automatic Control Engineering at the Technische Universität München, Germany, where she worked on patient-cooperative control strategies for rehabilitation robots. In May 2008, she joined the Sensory-Motor Systems Laboratory at the ETH Zürich, Switzerland. Her research interests include haptics, human motor control, and robotics. She is a Student Member of the IEEE.

Jan Veneman received M.Sc. degrees in mechanical engineering and philosophy of science, technology and society in 1998 and 2001, respectively, and the Ph.D. degree in biomechanical engineering in 2007, all from the University of Twente, Enschede, The Netherlands. His research project was on the design and evaluation of a prototype gait rehabilitation robot. His principal research interests are haptics, man–machine interaction, and robotics.

Edwin van Asseldonk received his M.Sc. degree (honors) in human movement sciences from the Free University, Amsterdam, The Netherlands and his Ph.D. degree in biomechanical engineering from the University of Twente in 2008. Currently, he is an assistant professor at the University of Twente. His field of research includes balance control, motor control in stroke patients and rehabilitation robotics.

Ralf Ekkelenkamp received his M.Sc. degree in electrical engineering at the University of Twente in 2003. From 2003 until 2007, he was working as a Ph.D. candidate on the advanced control of a gait rehabilitation robot, also at the University of Twente. Currently, he is a design engineer at Sensata Technologies.

Martin Buss received the diploma engineer degree in electrical engineering in 1990 from the Technical University Darmstadt, Germany, and the doctor of engineering degree in electrical engineering from the University of Tokyo, Japan, in 1994. In 2000, he finished his habilitation in the Department of Electrical Engineering and Information Technology, Technische Universität München, Germany. In 1988, he was a research student at the Science University of Tokyo, Japan, for one year. As a postdoctoral researcher, he worked at the Department of Systems Engineering, Australian National University, Canberra, Australia, in 1994–1995. From 1995 to 2000, he has been senior research assistant and lecturer at the Institute of Automatic Control Engineering, Department of Electrical Engineering and Information Technology, Technische Universität München, Germany. He has been appointed full professor, head of the control systems group, and deputy director of the Institute of Energy and Automation Technology, Faculty IV—Electrical Engineering and Computer Science, Technical University Berlin, Germany, from 2000–2003. Since 2003, he has been full professor (chair) at the Institute of Automatic Control Engineering, Technische Universität München, Germany. Since 2006, he has been the coordinator of the DFG Excellence Research Cluster Cognition for Technical Systems—CoTeSys. His research interests include automatic control, mechatronics, multimodal human–system interfaces, optimization, nonlinear, and hybrid discrete-continuous systems. He is a Member of the IEEE.

Herman van der Kooij received his Ph.D. degree with honors (cum laude) in 2000 and is an associate professor at the Department of Biomechanical Engineering at the University of Twente (0.8 fte), and Delft University of Technology (0.2 fte), The Netherlands. His expertise and interests are in the field of human motor control, adaptation, and learning, rehabilitation robots, diagnostic robotics, virtual reality, rehabilitation medicine, and neurocomputational modeling. He is a Member of the IEEE Engineering in Medicine and Biology Society Technical Committee of Biorobots and was a member of several scientific program committees in the field of rehabilitation robotics, biorobotics, and assistive devices. He is the founder and head of the Rehabilitation Robotics Laboratory, at the University of Twente, which developed powered exoskeletons for the rehabilitation of upper and lower extremities. He is also the founder and head of the Virtual Reality Human Performance Lab that combines robotic devices, motion capturing, and virtual environments to assess and train human balance, walking, and hand–eye coordination. He is a recipient of the VIDI award.

Address for Correspondence: Heike Vallery, Sensory Motor Systems Lab, ETH Zürich, 8008 Zürich, Switzerland. E-mail: heike.vallery@mavt.ethz.ch.

Authorized licensed use limited to: National Chung Hsing University. Downloaded on June 03,2010 at 07:55:47 UTC from IEEE Xplore. Restrictions apply.